THE JOURNAL OF BIOLOGICAL CHEMISTRY
Vol. 278, No. 20, Issue of May 16, pp. 18638–18648, 2003

Printed in U.S.A.

The C-terminal Domain of the Measles Virus Nucleoprotein Is Intrinsically Disordered and Folds upon Binding to the C-terminal Moiety of the Phosphoprotein*

Received for publication, January 16, 2003, and in revised form, March 3, 2003
Published, JBC Papers in Press, March 5, 2003, DOI 10.1074/jbc.M300518200

Sonia Longhi‡§, Véronique Receveur-Bréchot‡, David Karlin‡¶, Kenth Johansson‡‖, Hervé Darbon‡, David Bhella, Robert Yeo**, Stéphanie Finet‡‡, and Bruno Canard‡**

*From the ‡Architecture et Fonction des Macromolécules Biologiques, UMR 6098 CNRS et Université Aix-Marseille I et II, ESIL, Campus de Luminy, 13288 Marseille Cedex 09, France, **MRC Virology Unit, Institute of Virology, Church St., Glasgow G11 5JR, United Kingdom, and ‡‡European Synchrotron Radiation Facility, BP 220, 38043 Grenoble Cedex, France*

The nucleoprotein of measles virus consists of an N-terminal moiety, N_{CORE}, resistant to proteolysis and a C-terminal moiety, N_{TAIL}, hypersensitive to proteolysis and not visible as a distinct domain by electron microscopy. We report the bacterial expression, purification, and characterization of measles virus N_{TAIL}. Using nuclear magnetic resonance, circular dichroism, gel filtration, dynamic light scattering, and small angle x-ray scattering, we show that N_{TAIL} is not structured in solution. Its sequence and spectroscopic and hydrodynamic properties indicate that N_{TAIL} belongs to the premolten globule subfamily within the class of intrinsically disordered proteins. The same epitopes are exposed in N_{TAIL} and within the nucleoprotein, which rules out dramatic conformational changes in the isolated N_{TAIL} domain compared with the full-length nucleoprotein. Most unstructured proteins undergo some degree of folding upon binding to their partners, a process termed "induced folding." We show that N_{TAIL} is able to bind its physiological partner, the phosphoprotein, and that it undergoes such an unstructured-to-structured transition upon binding to the C-terminal moiety of the phosphoprotein. The presence of flexible regions at the surface of the viral nucleocapsid would enable plastic interactions with several partners, whereas the gain of structure arising from induced folding would lead to modulation of these interactions. These results contribute to the study of the emerging field of natively unfolded proteins.

Measles virus (MV)[1] is an enveloped RNA virus within the *Morbillivirus* genus of the *Paramyxoviridae* family. Its nonsegmented, negative sense, single-stranded RNA genome is packaged by the viral nucleoprotein (N) within a helical nucleocapsid. Transcription and replication are carried out on this (N·RNA) complex by the RNA-dependent RNA polymerase polymerase (L) associated with the phosphoprotein (P) (reviewed in Refs. 1 and 2). During genome replication, synthesis of viral RNA and encapsidation by N are concomitant (1, 2). However, N has the capacity to self-assemble on cellular RNA to form nucleocapsid-like particles in the absence of viral RNA and of any other viral protein (3–7). Therefore, a regulatory mechanism is necessary to prevent illegitimate self-assembly of N onto cellular RNA in the absence of ongoing genomic RNA synthesis. This role is played by P; association of P with the soluble, monomeric form of N (N°) prevents its illegitimate self-assembly (8–10). This soluble N°·P complex is the substrate used by the polymerase to initiate encapsidation of genomic RNA (10, 11). N forms complexes with P and with the P·L complex during transcription and replication also in its self-assembled form (N^{NUC}) (12–15).

Deletion analyses have shown that nucleoproteins of *Paramyxoviridae* are divided into two regions: a N-terminal moiety, N_{CORE}, well conserved in sequence, and a hypervariable, C-terminal moiety, N_{TAIL} (2) (see Fig. 1*A*). N_{CORE} contains all of the regions necessary for self-assembly and RNA binding (16, 17). Within N_{CORE}, deletion and mutational studies have shown that the central conserved region (MV; aa 258–357) and the aa 189–239 region, are involved in self-association and in RNA binding (4, 18–21). The precise location of RNA binding sites within N_{CORE} is unknown. The RNA binding site is probably formed by maturation of N during encapsidation, as suggested by the observation that all N mutants displaying an impaired self-association are not able to package RNA (4, 19, 21).

Within nucleocapsids, N_{TAIL} protrudes from the globular body of N_{CORE} (22, 23). In *Morbilliviruses* and *Respiroviruses*, the region responsible for binding of nucleocapsids to P is located within N_{TAIL} (13, 18, 20, 24). Consequently, N_{TAIL} is required for N·RNA to act as a template for viral RNA synthe-

* This work was supported in part by the CNRS. This study has been carried out with financial support from the Commission of the European Communities, specific program "Quality of Life and Management of Living Resources," QLK2-CT2001-01225, "Towards the Design of New Potent Antiviral Drugs: Structure-Function Analysis of *Paramyxoviridae* RNA Polymerase." The costs of publication of this article were defrayed in part by the payment of page charges. This article must therefore be hereby marked "*advertisement*" in accordance with 18 U.S.C. Section 1734 solely to indicate this fact.

§ To whom correspondence should be addressed: ESIL-CNRS-AFMB Case 925, 163, avenue de Luminy, 13288 Marseille Cedex 09, France. Tel.: 33-4-91-82-86-47; Fax: 33-4-91-82-86-46; E-mail: longhi@afmb.cnrs-mrs.fr.

¶ Supported by a grant from the Fondation pour la Recherche Médicale. Present address: Ecole de l'ADN, Association Grand Luminy, Case 922, Bât CCIMP, 13288 Marseille Cedex 09, France.

‖ Supported by a postdoctoral fellowship from the EMBO.

[1] The abbreviations used are: MV, measles virus; N, nucleoprotein; N°, soluble, monomeric form of N; P, phosphoprotein; L, RNA-dependent RNA polymerase; M, matrix protein; EM, electron microscopy; PCT, C-terminal moiety of P; PNT, N-terminal moiety of P; PMSF, phenylmethylsulfonyl fluoride; R_S, Stokes radius; R_SN, Stokes radius for a native protein; R_SU, Stokes radius for an unfolded protein; MM, molecular mass; *V*, hydrodynamic volume; DLS, dynamic light scattering; SAXS, small angle X-ray scattering; TFE, 2,2,2-trifluoroethanol; R_g, radius of gyration; IP, immunoprecipitation; *R*, mean net charge; *H*, mean hydrophobicity; IMAC, immobilized metal affinity chromatography; SeV, Sendai virus; mAb, monoclonal antibody; aa, amino acids.

sis (13, 16, 25). N_{TAIL} has also been shown to be required for stable binding of N° to P (16, 26).

Besides its role in encapsidating viral RNA, N also plays a role during viral assembly by interacting with the matrix protein (M) (27). The M-binding region of nucleocapsids has recently been mapped to N_{TAIL} in *Respiroviruses* (27), in agreement with the accessibility of N_{TAIL} on the surface of the nucleocapsid and with its net negative charge, which would favor the interaction with the highly positively charged M protein.

The fact that N_{TAIL} is not readily visualized by electron microscopy (EM) (28) and is hypersensitive to proteolysis (4, 28) strongly suggests that it is mostly unstructured within nucleocapsids, at least after isolation (29).

During the last decade, it has been shown that a considerable number of proteins (>100) have little or no ordered rigid structure under physiological conditions. These proteins are referred to as natively unfolded or "intrinsically disordered or unstructured" (for reviews, see Refs. 30–32). Conformational analysis has shown that natively unfolded proteins do not represent a uniform family, but rather they can be subdivided into two structurally distinct groups. The first group consists of proteins with extended hydrodynamic dimensions typical of random coils with no (or little) ordered secondary structure. The second group comprises the so-called premolten globules, which are more compact (but still less compact than globular or molten globule proteins) and conserve some residual ordered secondary structure (31, 32).

It has recently been proposed that the protein structure-function paradigm should be better replaced by the "protein quartet model" (31). According to this model, proteins can exist in any of the four thermodynamic states of proteins (ordered, molten globule, premolten globule, and random coil), and function can arise from any of these conformations and transitions between them. The functional importance of disorder may reside in advantages of flexible structures in comparison with rigid structures. In particular, an increased plasticity would (i) allow to couple a high specificity with a low affinity, (ii) enable binding of numerous structurally distinct targets, and (iii) provide the ability to overcome steric restrictions, enabling larger interaction surfaces in protein-protein and protein-ligand complexes than those obtained with rigid partners (31–35).

In this paper, we report the bacterial expression, purification, and characterization of MV N_{TAIL}. Using different, complementary biochemical and biophysical methods, we show that N_{TAIL} is intrinsically disordered and belongs to the premolten globule subfamily. We also show that N_{TAIL} is able to bind its physiological partner, P. Although there are intrinsically disordered proteins that carry out their function while being disordered from end to end (32), a majority folds in the presence of their physiological partner(s) (36, 37), a process known as "induced folding." We show that N_{TAIL} undergoes such an unstructured-to-structured transition upon binding to the C-terminal moiety of P (PCT).

EXPERIMENTAL PROCEDURES

Bacterial Strains and Media—The *Escherichia coli* strain XL1 Blue (Stratagene) was used for selection and amplification of DNA constructs. The *E. coli* strains BL21[DE3] and BL21 (Novagen) were used for expression of recombinant proteins. *E. coli* was grown in Luria-Bertani medium.

Chemicals and Antibodies—Restriction enzymes and T4 DNA ligase were purchased from NE Biolabs. *Pfu* polymerase was from Promega. Primers were purchased from Genosys. Nucleotide sequencing was carried out by Genome Express. The anti-hexahistidine tag monoclonal antibody (mAb) was purchased from Qiagen. The anti-N Cl 105 [2] and Cl 25 (38, 39) and the anti-P 49.21 mAbs (40) were kindly provided by D. Gerlier.

Plasmids—The plasmid pQE32/N_{TAIL}, encoding residues 400–525 of MV N (strain Edmonston B) with a hexahistidine tag fused to its N terminus was a kind gift of C. Rabourdin-Combe.

The plasmids pET21a/P_{H6} and pET21a/P encoding the MV P protein (strain Edmonston B) with or without an N-terminal hexahistidine tag, respectively, have been already described (41). The PCT gene construct, encoding the C-terminal moiety of P (PCT) (residues 231–507 of P) with a hexahistidine tag fused to its N terminus, was obtained by PCR, using pET21/P_{H6} as template. Forward primer (5′-GGCCCATATGCACCATCATCATCATCATGGCACAGACGCGAGATTAGCCTCAT-3′) was designed to introduce an *Nde*I restriction site fused to the N terminus of PCT, whereas reverse primer (5′-CCGGGAATTCTTACTTCATTATTATCTTCAT-3′) was designed to introduce an *Eco*RI site after the P stop codon. The PCR product was digested with *Nde*I and *Eco*RI, purified, and ligated between the *Nde*I and *Eco*RI sites of pET21a to yield pET21a/PCT_{H6}.

The plasmid pET21a/PNT_{H6}, encoding the N-terminal domain of P (PNT) (residues 1–230 of P) with an N-terminal hexahistidine tag, has been already described (41).

The plasmid pET21a/$N_{FLAG\text{-}H6}$, which encodes MV N with an N-terminal FLAG sequence (DYKDDDDK) (42) and a C-terminal hexahistidine tag, has already been described (4).

Expression of N_{TAIL} and PCT—E. coli strains BL21 and BL21[DE3] were used for the expression of pQE32/N_{TAIL} and of pET21a-derivative constructs, respectively. Since MV N and P genes contain several rare arginine codons (AGG) that are used with a very low frequency in *E. coli*, co-expression of N and P constructs with the plasmid pUBS520 (43), which supplies the corresponding rare tRNA, was carried out. Cultures were grown overnight to saturation in Luria-Bertani (LB) medium containing 100 μg/ml ampicillin and 50 μg/ml kanamycin. An aliquot of the overnight culture was diluted 1:25 in LB medium and grown at 37 °C. At A_{600} of 0.7, isopropyl β-D-thiogalactopyranoside was added to a final concentration of 0.2 mM, and the cells were grown at 37 °C for 3 h. The induced cells were harvested, washed, and collected by centrifugation. The resulting pellets were frozen at −20 °C.

Expression of tagged N, PNT, and untagged P was carried out as described in Refs. 25 and 48.

Purification of N_{TAIL} and PCT—The pellet containing N_{TAIL} was resuspended in 5 volumes (v/w) buffer A (50 mM sodium phosphate, pH 8, 300 mM NaCl, 10 mM imidazole, 1 mM phenylmethylsulfonyl fluoride (PMSF)) supplemented with 0.1 mg/ml lysozyme, 10 μg/ml DNase I, and protease inhibitor mixture (Sigma) (50 μl/g of cells). After a 20-min incubation with gentle agitation, the cells were disrupted by sonication (using a 750-watt sonicator and four cycles of 30 s each at 60% power output). The lysate was clarified by centrifugation at 30,000 × *g* for 30 min. Starting from a 1-liter culture, the clarified supernatant was incubated for 1 h with gentle shaking with 4 ml of chelating Sepharose Fast Flow Resin preloaded with Ni^{2+} ions (Amersham Biosciences), previously equilibrated in buffer A. The resin was washed with buffer A, and N_{TAIL} was eluted in buffer A containing 250 mM imidazole. Eluates were analyzed by SDS-PAGE for the presence of N_{TAIL}. The fractions containing N_{TAIL} were combined; diluted with 5 volumes of 50 mM sodium phosphate, pH 8, 1 mM PMSF; and incubated for 1 h with gentle shaking with 4 ml of Sepharose Q Fast Flow resin (Amersham Biosciences). The flow-through was recovered, filtered onto 0.8-μm filters (Pall Gelman Laboratories), and concentrated using a Centricon Plus-20 concentrator (molecular mass cut-off, 5000 Da) (Millipore Corp.). The protein was then loaded onto a Superdex 75 HR 10/30 column (Amersham Biosciences) and eluted in either 10 mM sodium phosphate, pH 7, or 10 mM Tris/HCl, pH 8, 5 mM EDTA. The protein was stored at −20 °C in the presence of 10% glycerol.

The pellet containing PCT was resuspended in 5 volumes (v/w) buffer B (10 mM Tris/HCl, pH 8, 300 mM NaCl, 10 mM imidazole, 10% glycerol, 1 mM PMSF) supplemented with 0.1 mg/ml lysozyme, 10 μg/ml DNase I, and protease inhibitor mixture (Sigma) (50 μl/g of cells). After a 20-min incubation with gentle agitation, the cells were disrupted by sonication, and the lysate was clarified as described above. Starting from a 1-liter culture, the clarified supernatant was incubated for 1 h with gentle shaking with 4 ml of Talon resin (Clontech), previously equilibrated in buffer B. The resin was washed with buffer B, and PCT was eluted in buffer B containing 50 mM EDTA. Eluates were analyzed by SDS-PAGE for the presence of PCT. The fractions containing PCT were combined, filtered onto 0.8-μm filters (Pall Gelman Laboratories), and concentrated using a Centricon Plus-20 concentrator (molecular mass cut-off, 5000 Da) (Millipore Corp.). The eluate from the affinity chromatography step was then loaded onto a Superdex 200 HR 10/30

[2] J. Chadwick and T. F. Wild, unpublished data.

column (Amersham Biosciences) and eluted in 10 mM Tris/HCl, pH 8, 300 mM NaCl, 5 mM EDTA, 10% glycerol, and 1 mM PMSF. The protein was stored at −20 °C.

Purification of PNT and of N were carried out as described in (25, 48). The 43-kDa N-terminal fragment of N, N_{CORE}, was obtained by limited trypsin digestion of N as described in Ref. 25, followed by gel filtration onto a Superdex 200 HR 10/30 column (Amersham Biosciences). N_{CORE} was eluted with 50 mM Tris/HCl, pH 7.5, 1 mM PMSF and stored at −20 °C in the presence of 20% glycerol.

All purification steps, except for gel filtrations, were carried out at 4 °C.

Apparent molecular mass of proteins eluted from gel filtration columns was deduced from a calibration carried out with low and high molecular weight calibration kits (Amersham Biosciences). The theoretical Stokes radii (R_S) of a native (R_SN) and fully unfolded (R_SU) protein with a molecular mass (MM) (in daltons) were calculated according to Ref. 44: $\log(R_S\text{N}) = 0.369 \times \log(\text{MM}) - 0.254$, and $\log(R_S\text{U}) = 0.533 \times \log(\text{MM}) - 0.682$. The hydrodynamic volume (V) was calculated from the Stokes radius as $V = 4/3\pi R_S^3$. The theoretical hydrodynamic volumes of a native (V_N), natively unfolded random coil (V_{NUcoil}), and natively unfolded premolten globule (V_{NUpmg}) protein of n residues were calculated according to Ref. 31: $\log(V_N) = (2.197 \pm 0.037) + (1.072 \pm 0.015) \times \log n$, $\log(V_{NUcoil}) = (1.997 \pm 0.078) + (1.498 \pm 0.035) \times \log n$, and $\log(V_{NUpmg}) = (2.33 \pm 0.12) + (1.234 \pm 0.047) \times \log n$.

Determination of Protein Concentration—Protein concentrations were calculated either using the theoretical absorption coefficients ϵ (mg/ml·cm) at 280 nm as obtained using the program ProtParam at the EXPASY server (available on the World Wide Web at www.expasy.ch/tools), or the Bio-Rad protein assay reagent (Bio-Rad).

Mass Spectrometry—Mass analysis of PCT was performed using a Voyager DE RP mass spectrometer (PerSeptive Biosystems). Samples (0.7 μl containing 15 pmol) were mixed with an equal volume of sinapinic acid matrix solution, spotted on the target, and then dried at room temperature for 10 min. The mass standard was apomyoglobin.

Mass analysis of tryptic fragments of N_{TAIL} was carried out by digesting (0.25 μg of trypsin) 1 μg of purified N_{TAIL} obtained after separation onto 12% SDS-PAGE. The experimental mass values of the tryptic fragments (determined as described above) were compared with theoretical values found in protein data bases (available on the World Wide Web at www.matrixscience.com and www.expasy.ch/cgi-bin/findmod0.pl). The mass standards were either autolytic tryptic peptides or keratin peptides.

Dynamic Light Scattering (DLS)—Dynamic light scattering experiments were performed with a Dynapro MSTC-200 (Protein Solutions) at 20 °C. All samples were filtered prior to the measurements (Millex syringe filters, 0.22 μm; Millipore Corp.). The hydrodynamic radius was deduced from translational diffusion coefficients using the Stokes-Einstein equation. Diffusion coefficients were inferred from the analysis of the decay of the scattered intensity autocorrelation function. All calculations were performed using the software provided by the manufacturer.

Two-dimensional NMR—A sample containing purified N_{TAIL} at a concentration of 0.5 mM in 10 mM sodium phosphate, pH 7, was used for the acquisition of a NOESY spectrum on a DRX500 Bruker spectrometer at 300 K with 2048 complex points in the directly acquired dimension and 512 complex points in the indirectly detected dimension. Solvent suppression was achieved by the WATERGATE 3-9-19 pulse (45). The data were processed using the UXNMR software; they were multiplied by a sine-squared bell and zero-filled to 1 K in the first dimension prior to Fourier transformation.

Circular Dichroism—The CD spectra were recorded on a Jasco 810 dichrograph using 1-mm thick quartz cells in 10 mM sodium phosphate, pH 7, at 20 °C. Structural variations of N_{TAIL} were measured as a function of changes in the initial CD spectrum upon the addition of either increasing concentrations of 2,2,2-trifluoroethanol (TFE) (Fluka) or different amounts of PCT, PNT, or lysozyme (Sigma). CD spectra were measured between either 185 and 260 nm or 190 and 260 nm at 0.2 nm/min and were averaged from three independent acquisitions. Mean ellipticity values per residue ([Θ]) were calculated as $[\Theta] = 3300\ m \times \Delta A/(lcn)$, where l represents path length (0.1 cm), n is the number of residues, m is the molecular mass in daltons, and c is the protein concentration expressed in mg/ml. Numbers of residues (n) are 139 for N_{TAIL}, 236 for PNT, 284 for PCT, and 129 for lysozyme, whereas m values are 15,300 Da for N_{TAIL}, 24,800 Da for PNT, 30,800 Da for PCT, and 14,300 Da for lysozyme. Protein concentrations of 0.1 mg/ml were used when recording individual spectra. Protein concentrations ranging from 0.1 to 0.15 mg/ml were used when recording spectra of protein mixtures. In this case, mean ellipticity values per residue ([Θ]) were calculated as $[\Theta] = 3300\ \Delta A/\{[(C_1n_1)/m_1) + (C_2n_2/m_2)]\ l\}$, where l represents path length (0.1 cm), n_1 or n_2 is number of residues, m_1 or m_2 is molecular mass in daltons, and c_1 or c_2 is protein concentration expressed in mg/ml for each of the two proteins in the mixture. The theoretical average ellipticity values per residue ($[\Theta]_{Ave}$) expected, assuming that neither any unstructured-to-structured transition nor any secondary structure rearrangement occurs, were calculated as follows: $[\Theta]_{Ave} = [([\Theta]_1n_1) + ([\Theta]_2n_2R)]/(n_1 + n_2R)$, where $[\Theta]_1$ and $[\Theta]_2$ correspond to the measured mean ellipticity values per residue, n_1 and n_2 to the number of residues for each of the two proteins, and R to the excess molar ratio of protein 2. The α-helical content was derived from the ellipticity at 220 nm as described in Ref. 46.

Small Angle X-ray Scattering (SAXS)—SAXS experiments were carried out on beamline ID2 (47) at the European Synchrotron Radiation Facility (Grenoble, France). Samples of purified N_{TAIL} (in buffer containing 10 mM Tris/HCl, pH 8, 5 mM EDTA, with 10% glycerol as radiation scavenger) were filtered prior each measurement (Millex syringe filters (0.22 μm); Millipore). The wavelength was 1.0 Å, and the sample-to-detector distance was 3.0 and 1.0 m, leading to scattering vectors q ranging from 0.02 to 0.20 $Å^{-1}$ and 0.05 to 0.40 $Å^{-1}$, respectively. The scattering vector is defined as $q = 4\pi/\lambda \sin\theta$, where 2θ is the scattering angle. The detector was an X-ray image intensified optically coupled to a FReLoN CCD camera developed by the European Synchrotron Radiation Facility. 40 successive frames of 0.7 s with a 5-s pause between each frame were recorded for each sample. The protein solution was circulated through an evacuated quartz capillary between each frame. Thus, no protein solution was irradiated longer than 0.7 s. Each frame was then carefully inspected to check for possible bubble formation or radiation-induced aggregation. No such effect was observed, and individual frames could then be averaged. Absolute calibration was made with a Lupolen sample. A series of measurements at different protein concentrations ranging from 1.8 to 9 mg/ml were performed to check for interparticle interaction. Background scattering was measured before or after each protein sample using the buffer solution and then subtracted from the protein scattering patterns after proper normalization and correction from detector response. All of the experiments were carried out at 8 °C.

The value of the radius of gyration (R_g) was derived from the Guinier approximation (48): $I(q) = I(0) \exp(-q^2R_g^2/3)$, where $I(q)$ is the scattered intensity and $I(0)$ is the forward scattered intensity. The radius of gyration and $I(0)$ are inferred from the slope and the intercept, respectively, of the linear fit of $Ln[I(q)]$ *versus* q^2 at low q values ($qR_g < 1.0$). The distance distribution function $P(r)$ is the histogram of all of the interatomic distances within a molecule. This function also provides the maximum dimension D_{max} of the molecule, which is defined as the point where $P(r)$ becomes zero. The $P(r)$ function was calculated by the Fourier inversion of the scattering intensity $I(q)$ using GNOM (49) and GIFT (50).

EM Studies—5 μl of protein suspension (at ~0.1 mg/ml) was loaded onto an air glow-discharged carbon-coated support grid for 30 s, washed in a 50-μl droplet of distilled H_2O, and then negatively stained with a 2% ammonium molybdate solution (pH 7.5). The structures formed by N and N_{CORE} were imaged in a JEOL 1200 EX II transmission electron microscope and recorded on Kodak SO163 film at × 30,000 magnification under low electron dose conditions.

To make accurate measurements of nucleocapsid dimensions, micrographs were digitized, on a Dunvegan Hi-Scan drum scanner (Dunvegan SA, Lausanne, Switzerland), at a raster step size of 10 μm/pixel, corresponding to 3.4 Å/pixel in the specimen. 200 top views of nucleocapsid rings were selected by cross-correlation of scanned micrographs against a ring model of the appropriate dimensions and excised into 90-$pixel^2$ boxes using the SPIDER image processing package (51). Rings were centered by cross-correlation against a ring model, and radial density profiles were calculated for each image. Average radial density profiles were calculated and plotted using ORIGIN (Microcal).

Immunoprecipitation (IP) Studies of N_{TAIL}—IP experiments were carried out using the anti-N mAbs Cl 25 and Cl 105 and bacterial lysates expressing either tagged N and N_{TAIL} or no recombinant protein. The different bacterial cultures were induced as described above, and 5-ml aliquots were pelleted and frozen at −20 °C.

The different aliquots were individually resuspended in 500 μl of buffer C (10 mM Tris/HCl, pH 8, 0.1% Igepal, 150 mM NaCl) and sonicated (using a 750-watt sonicator and three cycles of 7 s at 35% power output). The lysed aliquots were centrifuged for 10 min at 16,000 × g at 4 °C, and the supernatants, containing the soluble fractions, were recovered. Soluble fractions (50 μl) were mixed with 4 μg of either Cl 25 or Cl 105 anti-N mAb, 400 μl of buffer C were added in order to increase the volume during the binding step, and the mixtures

were incubated with 20 μl of Protein G-Sepharose resin (Amersham Biosciences) pre-equilibrated with buffer C. After a 1-h incubation with gentle agitation at 20 °C, the mixtures were centrifuged, and the resin was washed twice with 20 volumes of buffer C. It was then mixed with an equal volume of 2× Laemmli sample buffer, boiled, and loaded onto a 12% SDS-PAGE gel.

Binding of N_{TAIL} to P—5-ml aliquots of bacterial cultures expressing either N_{TAIL} or P induced as described above were harvested, and the cellular pellets were frozen at −20 °C.

An N_{TAIL} and a P aliquot were individually resuspended in 500 μl of buffer D (10 mM Tris/HCl, pH 8, 20 mM imidazole, 0.5 M NaCl) and sonicated (using a 750-watt sonicator and three cycles of 7 s at 35% power output). The lysed aliquots were clarified by centrifugation at 16,000 × *g* for 10 min at 4 °C, and the supernatants, containing the soluble fractions, were recovered. 250 μl of each of the two soluble fractions were mixed and immediately incubated with 50 μl of chelating Sepharose fast flow resin preloaded with Ni^{2+} ions (Amersham Biosciences), pre-equilibrated with buffer D. After a 1-h incubation at 20 °C with gentle agitation, the mixture was centrifuged, and the resin was washed five times with 10 volumes of buffer D. It was then mixed with 50 μl of 2× Laemmli sample buffer, boiled, and loaded onto a 12% SDS-PAGE gel.

Sequence Analysis and Secondary Structure Predictions—The accession number of MV N is P04851. Deviation in amino acid composition of N_{TAIL} and N_{CORE} were computed using the average amino acid frequencies of the SWISS-PROT data base (as obtained from the World Wide Web at us.expasy.org/sprot) as the reference value. The mean net charge (*R*) of a protein is determined as the absolute value of the difference between the number of positively and negatively charged residues divided by the total number of amino acid residues. It was calculated using the program ProtParam at the EXPASY server (available on the World Wide Web at www.expasy.ch/tools). The mean hydrophobicity (*H*) is the sum of normalized hydrophobicities of individual residues divided by the total number of amino acid residues minus 4 residues (to take into account fringe effects in the calculation of hydrophobicity). Individual hydrophobicities were determined using the Protscale program at the EXPASY server (available on the World Wide Web at www.expasy.ch/tools), using the options "Hphob/Kyte & Doolittle," a window size of 5, and normalizing the scale from 0 to 1. The values computed for individual residues were then exported to a spreadsheet, summed, and divided by the total number of residues minus 4 to yield *H*. $H_{Boundary}$ was computed as described by Uversky (31): $H_{Boundary} = (R + 1.15)/2.785$.

Secondary structure predictions were carried out using the JPRED program (available on the World Wide Web at on.ebi.ac.uk/servers/jpred.html) (52).

RESULTS

MV N is a modular protein composed of two regions: a well conserved N-terminal moiety, N_{CORE} (aa 1–399) and a hypervariable C-terminal moiety, N_{TAIL} (aa 400–525) (see Fig. 1*A*). The sequence variability and the sensitivity to proteolysis of N_{TAIL} (4, 28) are both hallmarks of intrinsic disorder (29, 53). We have thus analyzed the sequence properties of N_{TAIL} in order to check whether this domain possesses the features typical of intrinsically disordered proteins.

Domain Organization of N and Sequence Properties of N_{TAIL}—The amino acid composition of N_{TAIL} and the deviation from the average values in the SWISS-PROT data base are shown in Fig. 1*A*. N_{TAIL} has a peculiar composition, being depleted in all "order-promoting" residues (Trp, Cys, Phe, Tyr, Ile, Leu) and enriched in most "disorder-promoting" residues (Arg, Gln, Ser, and Glu), as already described for intrinsically disordered proteins (32) (Fig. 1*A*). Moreover, N_{TAIL} is predicted to be natively unfolded by the PONDR predictor of naturally disordered regions (54), as well by the method based on the mean hydrophobicity/mean net charge ratio (55) (data not shown). Finally, N_{TAIL} has little predicted secondary structure, a feature that has been recently noticed in protein regions with "no ordered regular structure" (56).

In order to directly investigate the structural properties of N_{TAIL}, we have expressed, purified, and characterized the N_{TAIL} domain alone.

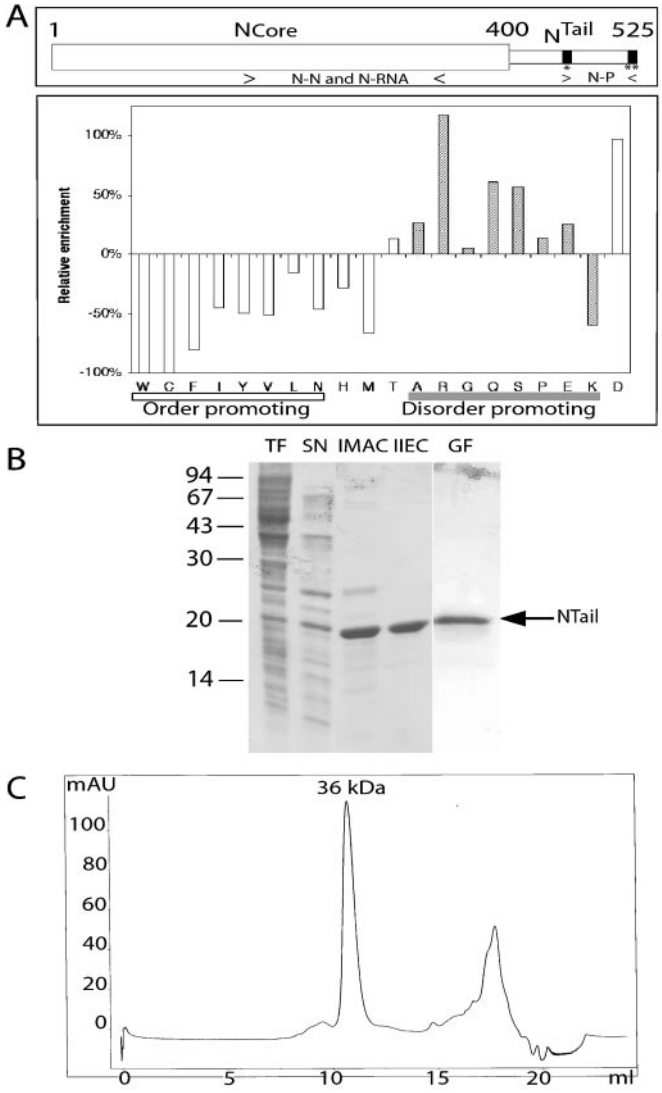

FIG. 1. *A*, domain organization of MV N and sequence composition of N_{TAIL}. *Top*, domain organization of N showing that it is composed of two regions, N_{CORE} (aa 1–399) and N_{TAIL} (aa 400–525). The epitopes recognized by the anti-N mAbs, Cl 25 mAb (aa 457–476) and Cl 105 mAb (aa 519–525), are *shaded* and indicated by *one* or *two asterisks*, respectively. The approximate location of the N-N, N-P, and RNA-binding regions are indicated *below N*. *Bottom*, deviation in amino acid composition from the average values in the Swiss-Prot data base of N_{TAIL}. The relative enrichment of order-promoting (*white bars*) and disorder-promoting residues (*shaded bars*) is shown. *B*, purification of N_{TAIL}. Coomassie Blue staining of a 12% SDS-PAGE. *TF*, bacterial lysate (total fraction); *SN*, clarified supernatant (soluble fraction); *IMAC*, eluent from immobilized metal affinity chromatography; *IIEC*, eluent from inverse ion exchange chromatography (nonretained fraction from ion exchange chromatography); *GF*, eluent from gel filtration. *C*, elution profile of N_{TAIL} from gel filtration. The main peak containing N_{TAIL} is *highlighted*, and the molecular mass deduced from the column calibration is shown.

Expression and Purification of N_{TAIL}—Most N_{TAIL} was recovered from the soluble fraction of bacterial lysates (Fig. 1*B*, *lane SN*). N_{TAIL} was purified to homogeneity (>95%) in three steps: immobilized metal affinity chromatography (IMAC), inverse ion exchange chromatography, and gel filtration (Fig. 1*B*). The identity of the recombinant product was confirmed by mass spectrometry analysis of the tryptic fragments obtained after digestion of purified N_{TAIL}. As shown in Fig. 1*B*, N_{TAIL} displays an abnormally slow migration in SDS-PAGE even after heat denaturation. In particular, it migrates with an apparent molecular mass (MM) of 20 kDa, whereas the expected MM is 15 kDa. This abnormal behavior has already been

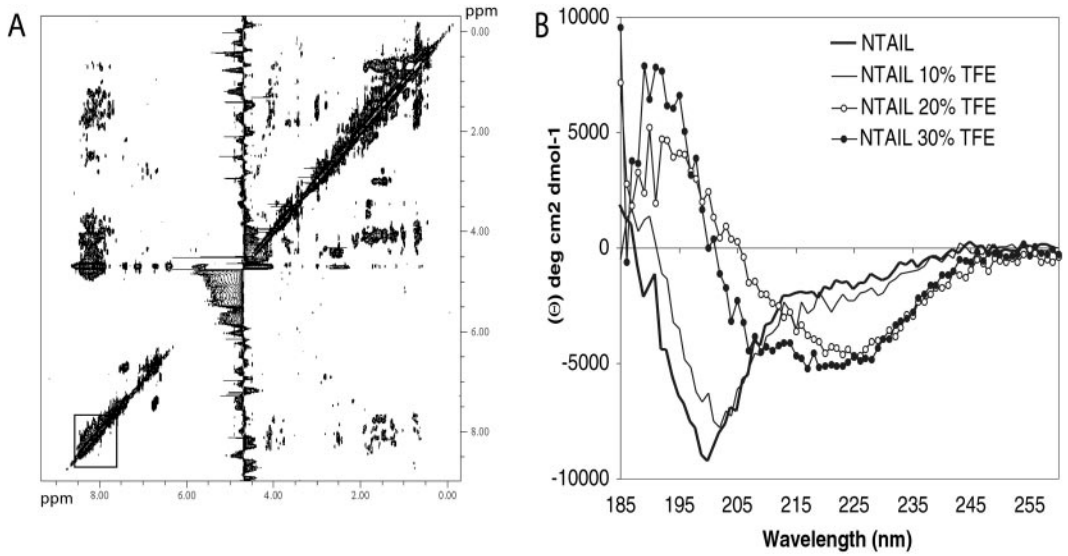

FIG. 2. *A*, NMR spectrum of N_{TAIL}. Two-dimensional ^1H NMR spectrum of a 0.5 mM solution of purified N_{TAIL} in 10 mM sodium phosphate, pH 7, at 283 K. *ppm*, values for resonance shifts in parts per million of the spectrophotometer frequency. The *frame* shows the small spread of the resonance frequencies for amide protons. *B*, CD spectrum of N_{TAIL}. Far-UV CD spectrum of N_{TAIL} in 10 mM sodium phosphate, pH 7, in the presence of increasing concentrations of TFE (0, 10, 20, and 30%).

observed in the case of the intrinsically disordered MV PNT (41) as well as in other intrinsically disordered proteins and can most likely be ascribed to their unusual sequence composition (30).

Size Exclusion Chromatography of N_{TAIL}—N_{TAIL} (15 kDa) is eluted from the gel filtration column as a peak corresponding to a 36-kDa globular protein (Fig. 1*C*). The same profile is obtained regardless of the nature of the buffer used and the presence of different NaCl concentrations (not shown), thus excluding the possibility that the observed behavior could be ascribed to nonspecific interactions of N_{TAIL} with the column matrix. The sharpness of the peak indicates the presence of a well defined species. The elution volume of a protein from a gel filtration column depends on its hydrodynamic properties. The hydrodynamic radius of a protein (Stokes radius (R_S)) can be deduced from its apparent MM (as seen by gel filtration) (44). The apparent MM of 36 kDa measured for N_{TAIL} corresponds to a Stokes radius of 27 ± 3 Å. On the other hand, the theoretical Stokes radius of a monomeric, native (R_SN) or fully unfolded (R_SU) protein can be estimated according to the equations described in Ref. 44. In the case of N_{TAIL}, R_SN = 19 Å and R_SU = 35 Å. Therefore, the Stokes radius experimentally measured for N_{TAIL} (27 Å) is not compatible with a monomeric, globular protein. Rather, such a large value of the Stokes radius can be attributed either to dimerization or to an extended conformation.

DLS Studies on N_{TAIL}—The hydrodynamic radius of proteins can also be derived by dynamic light scattering studies, since diffusion coefficients of proteins depend upon their size and shape. Globular proteins differ notably from fully or partly unstructured proteins in their hydrodynamic properties, and an empirical relationship between number of residues and hydrodynamic radius R_S has been established for native, globular proteins and for fully denatured proteins (57). The hydrodynamic radius measured for N_{TAIL} by DLS is R_S = 30 ± 2 Å, in either 10 mM sodium phosphate, pH 7, or 10 mM Tris/HCl, pH 8, 75 mM NaCl at a concentration of 1.25 mg/ml. This value is consistent (within the error bars) with the R_S value measured by gel filtration and corresponds to a hydrodynamic volume (*V*) of ~97,000 Å^3. According to the equations described by Uversky (31), the theoretical *V* expected for a native, globular protein composed of 139 residues is about 31,000 Å^3, whereas for a fully denatured protein it would be close to 180,000 Å^3. Thus, the *V* of N_{TAIL} calculated by DLS is about 3 times larger than the value expected for a globular protein and half of that expected for a denatured, fully unfolded protein. Rather, these hydrodynamic properties are consistent with the hypothesis that N_{TAIL} is a native premolten globule (31).

NMR Experiments on N_{TAIL}—In order to investigate its actual conformation, N_{TAIL} was studied by two-dimensional NMR spectroscopy. Fig. 2*A* shows the amide region of a NOESY spectrum. The very small spread of the resonance frequencies for amide protons (between 7.8 and 8.7 ppm; see *frame* in Fig. 2*A*) together with the scarcity of nuclear Overhauser effects in the amide-amide region are typical of a protein without any stable secondary structure. Moreover, the line width related to NH resonance frequencies is in accordance with the molecular size of a monomeric form of N_{TAIL}.

CD Studies on N_{TAIL}—The far-UV CD spectrum of N_{TAIL} at neutral pH is typical of an unstructured protein, as seen from its large negative ellipticity at 198 nm and very low ellipticity at 185 nm (Fig. 2*B*). However, the observed ellipticity values at 200 and 222 nm (−9700 and −2400 degrees cm^2 dmol^{-1}, respectively) (Fig. 2*B*) are consistent with the existence of some residual secondary structure, typical of the premolten globule state (39). Therefore, the spectroscopic and hydrodynamic parameters, together with the peculiar sequence properties of N_{TAIL}, converge to show that N_{TAIL} is mostly unstructured in solution and that it belongs to the class of natively unfolded or intrinsically disordered/unstructured proteins (37, 38, 42, 61, 62).

The majority of intrinsically disordered proteins folds upon binding to their physiological partner(s) (37). The solvent TFE mimics the hydrophobic environment experienced by proteins in protein-protein interactions and is therefore widely used as a probe to discover regions that have a propensity to undergo an induced folding (58). Thus, we recorded CD spectra of N_{TAIL} in the presence of increasing concentrations of TFE (Fig. 2*B*). N_{TAIL} shows an increasing gain of α-helicity upon the addition of TFE, as indicated by the characteristic maximum at 190 nm and minima at 208 and 222 nm (Fig. 2*B*). Most unstructured-to-structured transitions take place in the presence of 20% TFE, a concentration at which the α−helix content is estimated to be about 22% (using the ellipticity at 220 nm). The gain of

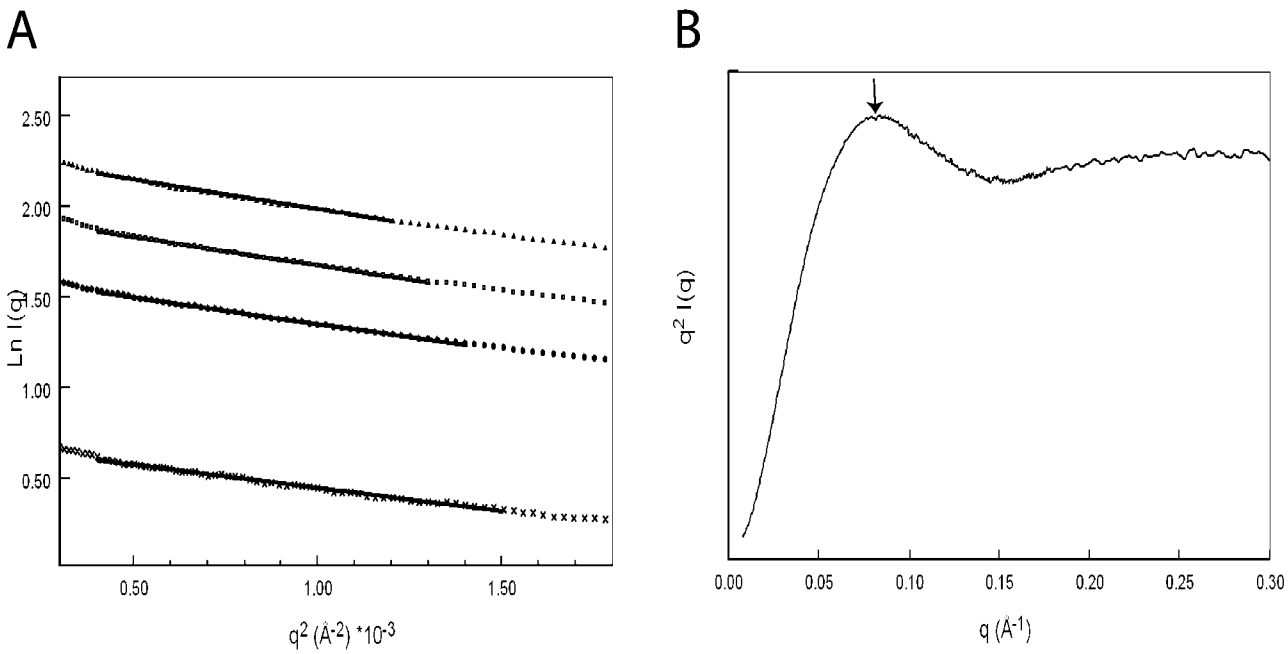

FIG. 3. **Small angle x-ray scattering experiments on N_{TAIL}.** *A*, Guinier plot of N_{TAIL} in 10 mM Tris, pH 8, 5 mM EDTA, 10% glycerol, at different protein concentrations: 9 mg/ml (*filled triangles*), 6.7 mg/ml (*open squares*), 4.5 mg/ml (*filled circles*), and 1.8 mg/ml (*crosses*). The slope of the straight lines (shown as a *thick line*) gives the value of R_g. The regression lines were fitted to the data within $qR_g < 1.0$. *B*, Kratky plot of the scattered intensity of N_{TAIL} at 9 mg/ml. The *arrow* indicates the bump at $q \approx 0.08$ Å^{-1}.

α-helicity induced by TFE, although already reported for other proteins, including MV PNT (41), is not a general rule; for instance, the acidic activator domain of GCN4 forms little or no α-helix in TFE concentrations as high as 30% and folds mostly as β-sheets in 50% TFE (59). In the case of N_{TAIL}, the use of TFE reveals a clear α-helix forming potential within this protein domain. Interestingly, this observation is in agreement with the secondary structure prediction made by the JPRED program (52), which predicts an α-helix (residues 489–504) as the only secondary structure element within N_{TAIL}.

SAXS Studies—SAXS studies are particularly well adapted to study flexible, low compactness or even extended macromolecules in solution. They provide low resolution structural data and give access to the mean particle size (radius of gyration, R_g) as well as to the maximal intramolecular distance (D_{MAX}). These two parameters give information on the degree of compactness of the molecule, and the latter gives an idea of the maximal degree of extension reached by the molecule in solution. Fig. 3*A* shows the Guinier plots of the SAXS data of N_{TAIL} at four different concentrations. Each curve can be well approximated by a straight line in the Guinier region ($qR_g < 1.0$). The slope gives the value of the radius of gyration, R_g, whereas the intercept of the straight line gives the $I(0)$, which is proportional to the MM of the scatterer. The R_g extrapolated at zero concentration is 27.5 ± 0.7 Å, and the deduced MM is 15,250 Da, which is in perfect agreement with the expected MM for a monomeric form (15,300 Da). A similar R_g value (26.9 ± 0.8 Å) has been obtained using the method based on the Debye function (60, 61). According to data already available in the literature (57, 62–64), the expected R_g of N_{TAIL} would be 15 Å for a globular protein and around 35–38 Å for a denatured, fully unfolded protein. Therefore, the observed R_g indicates that N_{TAIL} is not globular. However, the protein is more compact than a random coil, suggesting that it possesses some residual structure.

A very useful method to describe the structural properties of a molecule is the Kratky plot. In particular, one can from the shape of this plot infer the conformation adopted by the molecule. The Kratky plot of a globular protein has a typical bell shape with a clear maximum. For a completely unfolded protein or in a premolten globule conformation, no such maximum can be observed, and the curve displays a plateau (65). The Kratky plot of N_{TAIL} displays a bump at $q \approx 0.08$ Å^{-1} followed by a plateau for $q > 0.15$ Å^{-1} (see Fig. 3*B*). The absence of a maximum clearly indicates that N_{TAIL} is not globular and does not possess a tightly packed core. However, the observed bump may be indicative of some residual structure.

The distance distribution function, deduced from the scattering intensities of N_{TAIL} (data not shown), has a bell shape, with a maximum dimension D_{max} of 120–130 Å. This value, while being indicative of an extended, nonglobular conformation, is lower than expected for a random coil (62, 63).

All in all, the hydrodynamic properties of N_{TAIL} inferred from gel filtration, DLS and SAXS, indicate that N_{TAIL} adopts a typical nonglobular, premolten globule conformation in solution. Accordingly, it is more compact than a random coil and retains some residual secondary structure, in agreement with the CD studies. In conclusion, the spectroscopic and hydrodynamic properties of N_{TAIL}, together with its peculiar sequence composition, converge to show that it is a natively unfolded protein, belonging to the premolten globule subfamily.

Comparison of N and N_{CORE} by EM Studies—N produced in MV-infected cells (66) as well as recombinant MV N (4–6) forms nucleocapsids with a characteristic herringbone structure. In order to investigate whether the N_{TAIL} domain affects the conformation of N within nucleocapsids, we have analyzed by EM the nucleocapsid-like structures formed by either MV N or by a truncated form devoid of the N_{TAIL} moiety (N_{CORE}). N_{CORE} was obtained by limited proteolysis of purified N as described in Ref. 4, followed by gel filtration (data not shown).

EM analysis of full-length N reveals the presence of typical nucleocapsid-like, herringbone structures ranging in length from 20 to 80 nm (Fig. 4*A*, *left panel*, *arrows*). However, most of the nucleocapsid-like particles appear as rings with a mean diameter of 20 nm (Fig. 4*A*, *left panel*, *feathered arrows*). These rings correspond to shorter nucleocapsids viewed along their

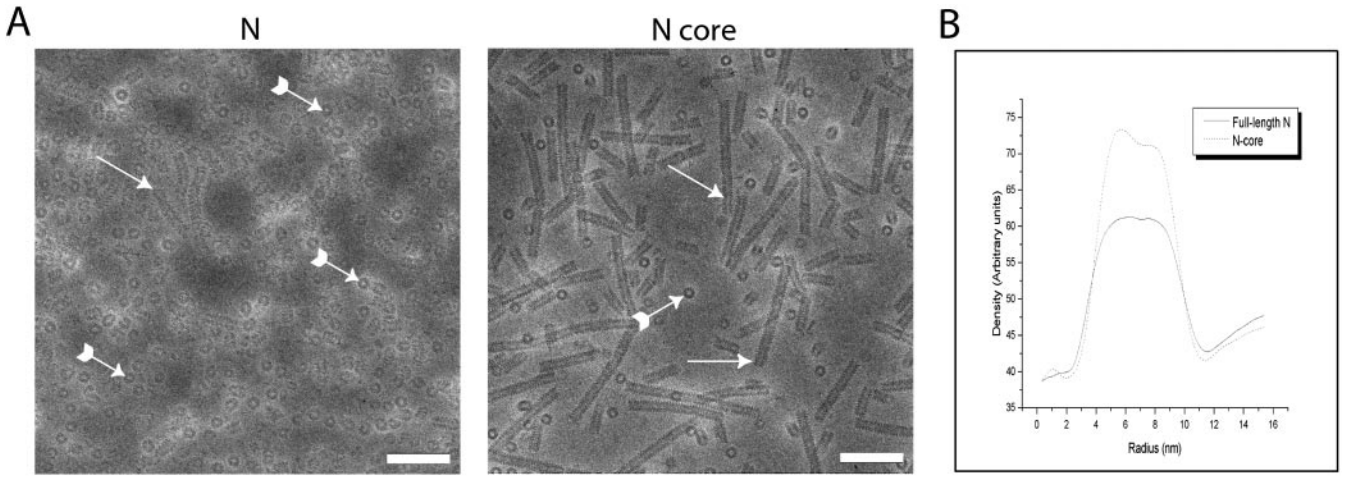

FIG. 4. **Negative staining EM studies of N and N_{CORE}.** *A*, negative stain electron micrographs of N and N_{CORE}. Nucleocapsid-like, herringbone structures are indicated by *arrows*. Rings (corresponding to short nucleocapsids viewed along their axis) are indicated by *feathered arrows*. *Bar*, 100 nm. *B*, average radial density profiles calculated from top views of ring structures composed of N and N_{CORE}.

axis, and their abundance suggests an intrinsic fragility in nucleocapsids formed by the bacterially expressed full-length nucleoprotein. Similar rings have also been described in Ref. 3.

Electron microscopy of N_{CORE}, however (Fig. 4*A*, *right panel*), reveals a predominance of rigid helices up to 400 nm long, as previously described (22, 23). This indicates that the removal of the exposed N_{TAIL} region appears to stabilize the interaction between turns of the helical nucleocapsid, either rendering it more robust or allowing short helices and rings to polymerize giving rise to longer helices. Radial density profiles, calculated from N and N_{CORE} rings (Fig. 4*B*), combined with visual inspection of negative stain images, reveals no obvious extra density in N, in agreement with previous data (22, 23). This suggests that N_{TAIL} is not visible as a distinct structural domain, because it is either poorly visualized due to its flexible nature or it is tightly associated with N_{CORE}, as has been demonstrated for the C terminus of rabies virus N (67).

The intrinsic flexibility of N_{TAIL} may sterically interfere with the formation of a stable interaction between successive turns of the helical nucleocapsid. The association of these rings gives rise to more rigid helical structures when imaged by negative stain EM. Therefore, the intrinsic disorder of N_{TAIL} provides a structural explanation for the observed gain of rigidity of N_{TAIL}-free nucleocapsids.

Epitope Exposure of N_{TAIL} and Binding to P—In order to check whether the isolated N_{TAIL} domain conserves a conformation similar to that adopted within the full-length N, we have performed IP studies using the anti-N Cl 25 and Cl 105 mAbs. These mAbs recognize the linear epitopes 457–476 and 515–525 of MV N, respectively. These mAbs are able to precipitate both N and N_{TAIL} from bacterial lysates (see Fig. 5*A*, *lanes N* and *Nt*), whereas no such bands are observed with a control bacterial lysate, thus confirming the specificity of the IP (see Fig. 5*A*, *lanes C*). Thus, these two epitopes are equally accessible within the full-length protein and within the isolated N_{TAIL} domain. This suggests that no dramatic conformational changes take place in the isolated N_{TAIL} domain compared with the full-length N.

As discussed above, MV N_{TAIL} is required for stable binding of N to P (18, 20, 26). To determine whether the isolated N_{TAIL} domain was able to bind P, we tested the ability of bacterial lysates expressing hexahistidine tagged N_{TAIL} to pull down untagged P onto an IMAC resin. The IMAC resin selectively pulled down N_{TAIL} expressed alone but not the untagged P expressed alone (Fig. 5*B*, *lanes Nt* and *P*). When both lysates were mixed, the IMAC resin selectively pulled down N_{TAIL} together with an additional protein that has the same electrophoretic mobility of P (Fig. 5*B*, *lane Nt + P*). The identity of this protein band was confirmed by Western blotting using an anti-P mAb (data not shown), thus proving that the N_{TAIL} domain on its own is able to bind its physiological partner in bacterial lysates.

P, the Physiological Partner of N_{TAIL}—As already mentioned, a large majority of natively unfolded proteins or protein domains characterized so far undergo disorder-to-order transitions in the presence of their physiological partner(s) (32, 33, 35, 37). The availability of the physiological partner of N_{TAIL} enables us to check for the occurrence of such unstructured-to-structured transitions.

The P protein of MV consists of an N-terminal moiety (aa 1–230), PNT, responsible for binding to N_{CORE} within the N°·P complex (26), and of a C-terminal moiety (aa 231–507), PCT, responsible for binding to N_{TAIL} in both N°·P and N^{NUC}·P complexes (9, 68). We have recently shown that the PNT domain of MV P is intrinsically disordered when expressed alone (41) and probably also in the context of full-length P.[3] Therefore, the interaction between N_{TAIL} and P may result in a possible induced folding of PNT concomitantly to the possible induced folding of N_{TAIL}. Since the purified PNT domain was already available (41), we purified the PCT moiety in order to monitor the possible structural transitions of N_{TAIL} in the presence of either PNT or PCT.

Most bacterially expressed PCT is found in the soluble fraction of the bacterial lysate (data not shown). Purification consists of two steps, IMAC followed by gel filtration. The expected MM of the purified product (31 kDa) was confirmed by mass spectrometry. However, PCT migrates in SDS-PAGE as a 36-kDa protein (see Fig. 5*C*). This discrepancy may be due to the presence of a region (aa 231–307 of P) of peculiar composition (rich in Gly, Ser, Ala, and Glu) at the N terminus of PCT. Although PCT is eluted from the gel filtration column as a very broad peak (not shown), DLS studies have shown the presence of a major (97%) species with a MM of ~200 kDa. This MM may correspond either to a high degree of oligomerization or to a very elongated shape of the protein or to both, as in the case of Sendai virus (SeV) PCT (69).

The eluent from the gel filtration column (see Fig. 5*C*) contains several protein species. Western blot analysis with an anti-hexahistidine tag mAb (not shown) showed that the dif-

[3] S. Longhi, K. Johansson, D. Karlin, and B. Canard, unpublished data.

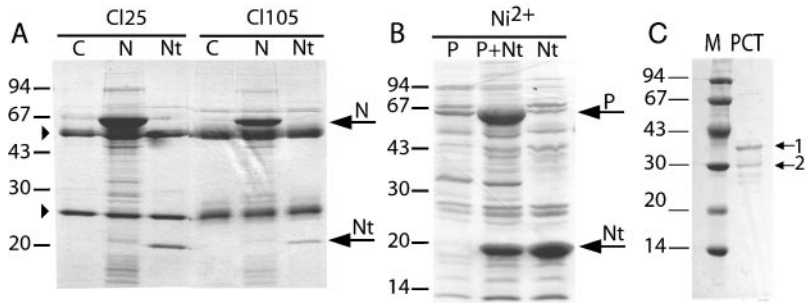

FIG. 5. *A*, IP of N and N_{TAIL} by the Cl 25 and Cl 105 mAbs. Coomassie Blue staining of a 12% SDS-PAGE. *Lanes N* and *Nt*, IP of tagged N and N_{TAIL} from bacterial lysates. *Lanes C*, IP from a control bacterial lysate expressing no recombinant protein. The *arrowheads* show the light and heavy chains of the mAb, which are visible on the gel around 25 and 55 kDa, respectively. *B*, binding of N_{TAIL} to P. Coomassie Blue staining of a 12% SDS-PAGE. Pull-down onto IMAC resin of untagged P (*P*), tagged N_{TAIL} (*Nt*), and untagged P plus tagged N_{TAIL} (*P + Nt*). *C*, purification of PCT. Coomassie Blue staining of a 12% SDS-PAGE. *M*, molecular mass markers; *PCT*, purified (*IMAC + GF*) PCT. *Arrows 1* and *2* indicate the full-length and the truncated form of PCT, respectively.

ferent protein bands are degradation products. Among the different products, two major bands are present (see the *arrows* in Fig. 5*C*), the lower of which corresponds to a truncated form devoid of an 8-kDa C-terminal fragment (see *arrow 2* in Fig. 5*C*). Mass spectrometry analysis of PCT allowed the precise identification of the cleavage site at position 436 of P, thus indicating that this region is flexible and exposed to the solvent.

Does N_{TAIL} Undergo an Induced Folding in the Presence of PCT?—To monitor possible structural transitions of N_{TAIL} in the presence of PCT, we have used far-UV CD spectroscopy.

The CD spectrum of purified PCT (see Fig. 6*A*, *gray line*) is typical of a protein with a predominant α-helical content, as seen by the positive ellipticity between 185 and 200 nm and by two minima at 208 and 222 nm. The α-helical content (estimated as 37% based on the ellipticity at 220 nm) is in agreement with structural data on SeV PCT domains (70, 71). After mixing N_{TAIL} with different molar excesses of PCT, the observed CD spectra of the mixtures differ from the corresponding theoretical average curves calculated from the individual spectra. Since the theoretical average curves correspond to the spectra that would be expected if no structural variations occur, deviations from these curves point out structural transitions. Most pronounced structural transitions are observed with an N_{TAIL}/PCT molar ratio of 1:1.5 (Fig. 6*A*). When equimolar amounts are used, only slight deviations from the theoretical average curve are observed; the two spectra are almost perfectly superimposable except for the 185–195-nm region, in which a 30% increase of ellipticity is observed (data not shown). In the presence of molar excesses of PCT, a random coil to α-helix transition can be observed, as indicated by the much more pronounced minima at 208 and 222 nm and by the higher ellipticity at 190 nm of the experimentally observed spectra compared with the corresponding theoretical average curves (Fig. 6*A*). Moreover, the α-helical contents of the mixtures (ranging from 38 to 48% at different molar ratios, with the highest value being obtained with a 1.5-fold excess of PCT) are not only higher than those of the corresponding theoretical average curves, but are also higher than the α-helical content of PCT alone. Gradually increasing the concentrations of PCT to molar ratios as high as 5 does not result in more drastic structural variations than those observed at a 1.5-fold molar excess of PCT (data not shown).

As a control, we recorded CD spectra of lysozyme either alone or mixed with N_{TAIL} at different molar ratios. As shown in Fig. 6*B* (*gray line*), the lysozyme spectrum is typical of an α/β protein, in agreement with structural data (72). Mixing equimolar amounts of the two proteins does not result in any significant structural variations. The experimentally measured CD spectrum of the mixture is in fact superimposable on the theoretical average curve (see Fig. 6*B*), as expected if no interaction occurs between lysozyme and N_{TAIL}. The same results were obtained at a 5-fold excess of lysozyme (data not shown).

As shown in Fig. 6*C*, no significant structural variations are observed with equimolar amounts of N_{TAIL} and PNT, with all spectra being typical of unfolded proteins. The same results were obtained by gradually increasing the amounts of PNT to molar excesses as high as 5 (data not shown). These results can be accounted for by assuming either that the two proteins do not interact, in agreement with the results reported in the literature (9, 68), or that the interaction does not imply any concomitant unstructured-to-structured transition.

The quite good superimposition between experimental and theoretical curves observed when mixing N_{TAIL} with either PNT or lysozyme (both at different molar excesses) confirms the significance of the deviation observed in the case of the N_{TAIL}-PCT mixtures (see Fig. 6*A*). Therefore, these results indicate that N_{TAIL} undergoes an induced folding upon binding to PCT.

A pioneering study has recently demonstrated that an intrinsically disordered protein region is in fact structured in living cells (73). FlgM, a 97-residue protein from *Salmonella typhimurium*, which regulates flagellar synthesis by binding the transcription factor σ^{28}, is fully unstructured *in vitro* (74). However, NMR performed on living *E. coli* overexpressing FlgM showed that the C terminus of FlgM is in fact structured *in vivo*, in the same manner as it becomes structured upon binding to σ^{28} *in vitro*, whereas its N terminus remains unstructured. Furthermore, the same gain of structure is observed *in vitro* in the presence of >400 g/liter glucose (73).

In order to check whether such solute-induced structural transitions could be observed also in the case of N_{TAIL}, we have recorded a CD spectrum of N_{TAIL} in the presence of 440 g/liter glucose (Fig. 6*D*). As shown in Fig. 6*D*, the spectrum obtained is still characteristic of an unfolded protein, and is similar to the spectrum obtained in the absence of glucose. According to Dedmon *et al.* (73), these results suggest that N_{TAIL} would belong to the class of intrinsically disordered proteins that "do not become structured at physiologically relevant solute concentrations" and that require a physiological partner to fold.

DISCUSSION

The high proteolytic sensitivity of N_{TAIL}, together with its peculiar sequence properties, strongly suggests that it is mostly unstructured.

The hydrodynamic properties of N_{TAIL} inferred from both gel filtration and DLS experiments are consistent with N_{TAIL} being either a stable globular dimer or a monomeric, extended

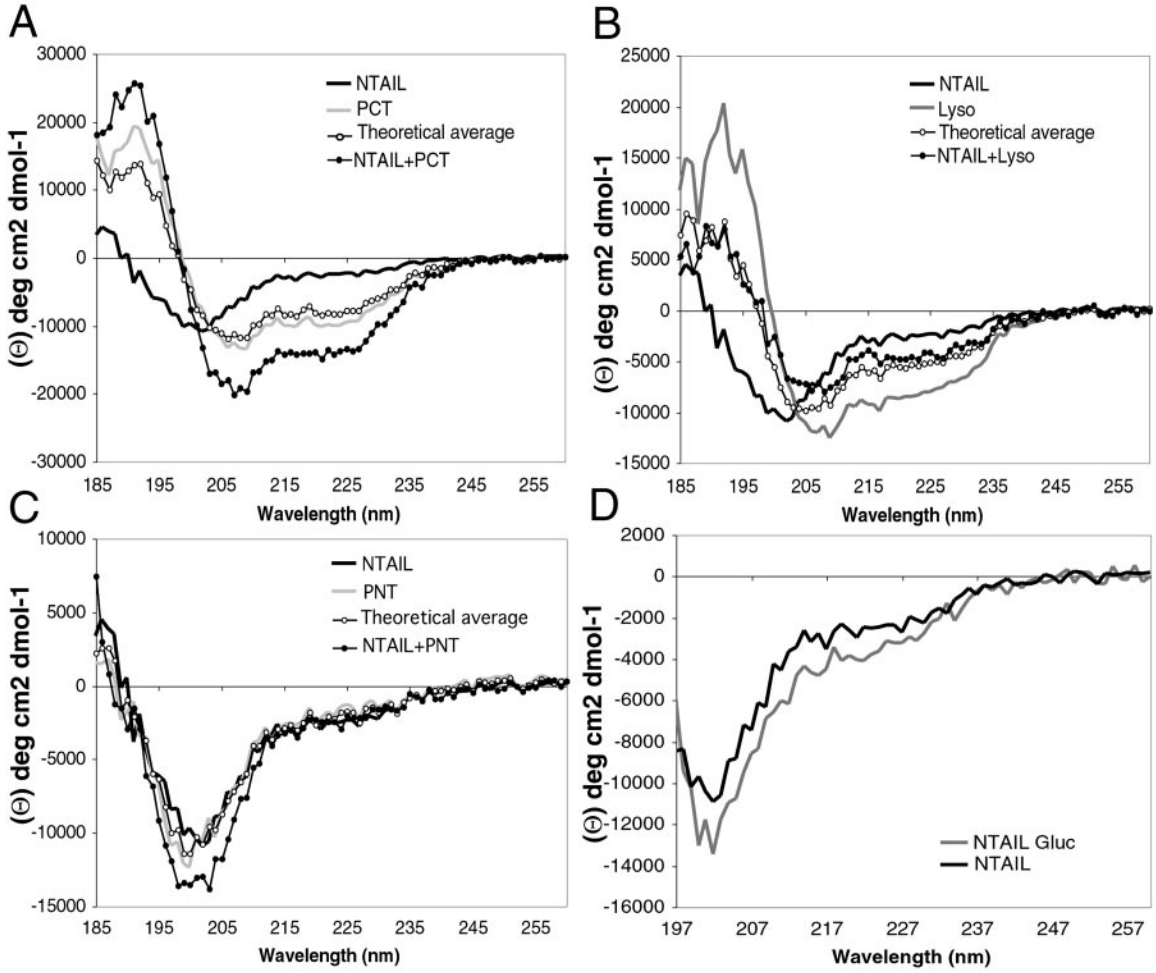

FIG. 6. **Induced folding of N_{TAIL}.** *A*, CD spectra of N_{TAIL}, PCT, and a 1:1.5 molar mixture of N_{TAIL} + PCT. *B*, CD spectra of N_{TAIL}, lysozyme, and an equimolar mixture of N_{TAIL} + lysozyme. *C*, CD spectra of N_{TAIL}, PNT, and an equimolar mixture of N_{TAIL} + PNT. The theoretical average curves calculated by assuming that no structural variations occur (see "Experimental Procedures") are also shown. *D*, CD spectra of N_{TAIL} in the absence (*NTAIL*) and in the presence (*NTAIL Gluc*) of 440 g/liter glucose. Only the region between 197 and 260 nm is shown, due to a strong absorption of glucose in the extreme far-UV region.

protein. Using NMR and CD, we show that N_{TAIL} is monomeric and mostly unstructured. However, its far-UV spectroscopic parameters indicate that N_{TAIL} is not fully unfolded, but rather it conserves a residual secondary structure content typical of natively unfolded proteins with a premolten globule conformation (31).

The scattering patterns obtained by SAXS show that N_{TAIL} is a nonglobular protein. However, it retains a certain degree of compactness, as seen by the R_g and D_{max} values. The structural properties of the polypeptide chain can also be determined by the R_S/R_g ratio. This ratio should be $(3/5)^{1/2}$ for a globular protein, around 0.9 for a premolten globule, and ~1.5 for a random coil (75). In the case of N_{TAIL}, the R_S and R_g values obtained by DLS and SAXS, respectively, lead to a ratio of 1.1, which is consistent with a premolten globule. Moreover, the mean hydrodynamic volume inferred from gel filtration and DLS studies (~97,000 Å^3) is in agreement with the value expected for a native premolten globule (about 94,000 Å^3) (31).

In addition, N_{TAIL} lies in a region of the hydrophobicity *versus* net charge plot, which is typical of native premolten globules (31). In particular, intrinsic coils are more distant from the border between rigid and intrinsically unstructured proteins than intrinsic premolten globules. In the case of N_{TAIL}, the distance value from the border ($H_{boundary} - H$) is 0.05 (see under "Experimental Procedures"), which is consistent with the value expected for a native premolten globule (0.037 ± 0.033) (31).

Thus, N_{TAIL} can be described as a nonglobular polypeptide chain, more compact than a random coil, containing a significant amount of residual structure. This residual structure may prevent the polypeptide chain from adopting multiple conformations. In agreement, the distribution of the conformations of N_{TAIL} is narrow, as seen by the relative sharpness of the elution peak observed in gel filtration, compared with what would be expected for a fully denatured protein in the presence of chaotropic agents (urea, guanidinium chloride). The residual ordered secondary structure of N_{TAIL} may arise from dynamic breaking and reforming of interactions. We can reasonably speculate that these residual interactions could enable a more efficient start of the folding process induced by a binding partner.

The intrinsic disorder of N_{TAIL} provides a possible structural explanation for the observed increase in rigidity of N_{TAIL}-free nucleocapsids. The removal of the N_{TAIL} region by limited proteolysis leads to a more rigid nucleocapsid, as indicated by the fact that EM micrographs of N_{CORE} mostly contain herringbone structures, as opposed to EM images of N, which mainly contain rings. The presence of flexible regions at the surface of the viral nucleocapsid would ideally enable the viral ribonucleoproteic complex to have plastic interactions with several partners, such as the polymerase complex (L·P) but also possibly components of the cell cytoskeleton (76, 77). Striking changes in nucleocapsid conformation in response to either

increasing salt concentrations or limited proteolysis have already been described (22, 23, 78) and point out the plasticity of its helical structure. This plasticity suggests that changes in the microenvironment of the nucleocapsid could affect its conformation during viral RNA transcription and replication, or during virus assembly, processes in which modifications in the coiling of the nucleocapsid could be important.

Most natively unfolded proteins or protein domains characterized so far undergo some degree of folding in the presence of a physiological partner (see Refs. 32, 33, 35, and 37). After showing that N_{TAIL} alone still conserves the ability to bind P, we have studied by far-UV spectroscopy the possible structural transitions of N_{TAIL} in the presence of PCT and PNT. CD is the method of choice to monitor such structural variations, since a residual structural content as low as 10–20% can be determined by this method. Indeed, this method turned out to be sensitive enough to detect unstructured-to-structured transitions upon binding of N_{TAIL} to PCT, whereas no structural transitions were detected in the presence of either PNT or lysozyme. In particular, binding of N_{TAIL} to PCT results in a strong unstructured-to-structured transition rather than in minor local structural changes, as shown by the considerable gain of α-helicity of the mixture (48%) compared with PCT (37%). The gain of α-helicity of N_{TAIL} observed in the presence of different molar excesses of PCT is in agreement with the strong α-helical propensity of N_{TAIL} pointed out in experiments using TFE. The highest α-helical content has been obtained with a 1.5-fold excess of PCT. A possible interpretation for this result may come from analysis of purified PCT. As shown in Fig. 5*C*, purified PCT consists of two major bands: a full-length form and a truncated form devoid of the last 70 C-terminal residues, the relative abundance of which can be roughly estimated to be 70 and 30%, respectively. Biochemical data on SeV have shown that the extreme C terminus (aa 479–568) of PCT contains the region responsible for binding to N (79, 80). Accordingly, it is possible that in the purified PCT sample only the upper band may participate to the interaction with N_{TAIL}. Therefore, a 1.5-fold excess of PCT may indeed correspond to an equimolar ratio between N_{TAIL} and a form of PCT able to make a productive interaction. On the other hand, in the presence of lower amounts of PCT, such as those used in the equimolar mixture, only very slight structural transitions are observed, even if 70% of N_{TAIL} is expected to be complexed to PCT. Thus, the gain of structure of N_{TAIL} does not seem to take place gradually but rather follows a cooperative transition, where the midpoint transition is just below 1.5-fold molar excess of PCT. Such a cooperative transition is typical of protein folding/unfolding processes. Increasing the molar excess of PCT beyond 1.5-fold does not result in any stronger unstructured-to-structured transitions. This may reflect the formation of a 1:1 stoechiometric complex. Therefore, at concentrations of PCT above those required for the formation of such a complex, no more N_{TAIL} would be available for binding to PCT, and saturation of the system would be achieved.

These results indicate that N_{TAIL} folds upon binding to its physiological partner, P. However, the possibility that the observed disorder-to-order transitions may also concern flexible regions within PCT is an open question. In this regard, indications are expected to arise from further structural studies, in particular crystallographic studies of N_{TAIL}-PCT complexes. In addition, we point out that the studies presented in this paper do not allow us to answer the question as to whether the gain of structure of N_{TAIL} takes place in the N^{NUC}·P or in the N°·P complex, or in both. Further studies are required to discriminate among these possibilities.

The intrinsic disorder is abundant within the replicative complex of MV, as indicated by experimental evidence accumulated on PNT and N_{TAIL}. Furthermore, in this paper, we report biochemical evidence suggesting that MV P possesses an additional flexible region, as indicated by the protease sensitivity observed within PCT. These results are in agreement with biochemical and structural data on SeV P, indicating the presence of a flexible linker, sensitive to proteolysis within the 447–517 region (69–71).

One advantage of unstructured regions of proteins might be their ability to bind to a wide variety of structurally distinct substrates with a weak affinity (32, 35). The pattern of interactions of N_{TAIL} is consistent with this hypothesis; N_{TAIL} takes part in numerous interactions with different protein partners, including P (both within N°·P and N^{NUC}·P), the polymerase complex P·L, M (27), the interferon regulatory factor 3 (81), and possibly components of the cell cytoskeleton (76, 77). Moreover, N_{TAIL} within viral nucleocapsids released from infected cells also binds to the human immunoglobulin G receptor FcγRII, provoking partial immunosuppression (82, 83). Finally, a conserved, hydrophobic patch at the extreme C terminus of *Morbillivirus* N_{TAIL} has been described to bind to the heat-shock protein Hsp72, which modulates the level of viral RNA synthesis (25). This is coherent with the proposal that in addition to their function of promoting protein folding, some chaperones bind hydrophobic patches in intrinsically disordered proteins, modulating their accessibility and/or their sensitivity to proteolysis (32).

N_{TAIL} plays very different roles during viral replication, being involved in RNA transcription, RNA replication, and viral assembly. One role of N_{TAIL} in actively replicating nucleocapsids could be to put into contact several proteins within the replicative complex, such as the N°·P and the P·L complexes. One can speculate that the gain of structure of N_{TAIL} upon binding to its physiological partner could result in stabilization of the N·P complex. The increased rigidity of N_{TAIL} would lead to a decrease in the number of conformations adopted by N_{TAIL} in solution and thereby to an increased affinity for its target. At the same time, folding of N_{TAIL} would result in a modification in the pattern of solvent-accessible regions, resulting in the shielding of specific regions of interaction. As a result, N_{TAIL} would no longer be available for binding to its other partners.

This paper provides new perspectives in the study of disordered regions within the MV replicative complex; in particular, the gain of structure arising from the interaction with the physiological partner may lead to protein complexes rigid enough to allow crystallization. The crystal structure determination of such complexes would represent an important step toward the understanding of the molecular mechanism of N and P.

Acknowledgments—We thank M. C. Trescol-Biémont and C. Rabourdin-Comble for kindly providing the plasmid encoding N_{TAIL}, A. Mosbah for help with the NMR study, M. Desmadril for critical advice with CD, and D. Gerlier for the anti-N and anti-P monoclonal antibodies. We thank D. Gerlier and J. Curran for critical reading of the manuscript. We thank K. Dunker for useful discussions.

REFERENCES

1. Curran, J., and Kolakofsky, D. (1999) *Adv. Virus Res.* **54,** 403–422
2. Lamb, R. A., and Kolakofsky, D. (2001) in *Fields Virology* (Fields, B. N., Knipe, D. M., and Howley, P. M., eds) 4th Ed., pp. 1305–1340, Lippincott-Raven, Philadelphia, PA
3. Warnes, A., Fooks, A. R., Dowsett, A. B., Wilkinson, G. W., and Stephenson, J. R. (1995) *Gene* (*Amst.*) **160,** 173–178
4. Karlin, D., Longhi, S., and Canard, B. (2002) *Virology* **302,** 420–432
5. Fooks, A. R., Stephenson, J. R., Warnes, A., Dowsett, A. B., Rima, B. K., and Wilkinson, G. W. (1993) *J. Gen. Virol.* **74,** 1439–1444
6. Bhella, D., Ralph, A., Murphy, L. B., and Yeo, R. P. (2002) *J. Gen. Virol.* **83,** 1831–1839
7. Spehner, D., Kirn, A., and Drillien, R. (1991) *J. Virol.* **65,** 6296–6300
8. Spehner, D., Drillien, R., and Howley, P. M. (1997) *Virology* **232,** 260–268
9. Huber, M., Cattaneo, R., Spielhofer, P., Orvell, C., Norrby, E., Messerli, M.,

Perriard, J. C., and Billeter, M. A. (1991) *Virology* **185,** 299–308
10. Curran, J., Marq, J. B., and Kolakofsky, D. (1995) *J. Virol.* **69,** 849–855
11. Horikami, S. M., Curran, J., Kolakofsky, D., and Moyer, S. A. (1992) *J. Virol.* **66,** 4901–4908
12. Ryan, K. W., and Portner, A. (1990) *Virology* **174,** 515–521
13. Buchholz, C. J., Retzler, C., Homann, H. E., and Neubert, W. J. (1994) *Virology* **204,** 770–776
14. Curran, J. (1996) *Virology* **221,** 130–140
15. Curran, J. (1998) *J. Virol.* **72,** 4274–4280
16. Curran, J., Homann, H., Buchholz, C., Rochat, S., Neubert, W., and Kolakofsky, D. (1993) *J. Virol.* **67,** 4358–4364
17. Buchholz, C. J., Spehner, D., Drillien, R., Neubert, W. J., and Homann, H. E. (1993) *J. Virol.* **67,** 5803–5812
18. Liston, P., Batal, R., DiFlumeri, C., and Briedis, D. J. (1997) *Arch. Virol.* **142,** 305–321
19. Myers, T. M., Smallwood, S., and Moyer, S. A. (1999) *J. Gen. Virol.* **80,** 1383–1391
20. Bankamp, B., Horikami, S. M., Thompson, P. D., Huber, M., Billeter, M., and Moyer, S. A. (1996) *Virology* **216,** 272–277
21. Myers, T. M., Pieters, A., and Moyer, S. A. (1997) *Virology* **229,** 322–335
22. Heggeness, M. H., Scheid, A., and Choppin, P. W. (1980) *Proc. Natl. Acad. Sci. U. S. A.* **77,** 2631–2635
23. Heggeness, M. H., Scheid, A., and Choppin, P. W. (1981) *Virology* **114,** 555–562
24. Ryan, K. W., Portner, A., and Murti, K. G. (1993) *Virology* **193,** 376–384
25. Zhang, X., Glendening, C., Linke, H., Parks, C. L., Brooks, C., Udem, S. A., and Oglesbee, M. (2002) *J. Virol.* **76,** 8737–8746
26. Harty, R. N., and Palese, P. (1995) *J. Gen. Virol.* **76,** 2863–2867
27. Coronel, E. C., Takimoto, T., Murti, K. G., Varich, N., and Portner, A. (2001) *J. Virol.* **75,** 1117–1123
28. Deshpande, K. L., and Portner, A. (1984) *Virology* **139,** 32–42
29. Hubbard, S. J., Beynon, R. J. (2001) in *Proteolytic Enzymes* (Beynon, R. J., and Bond, J. D., eds) 2nd Ed., pp. 233–264, Oxford University Press, Oxford, UK
30. Tompa, P. (2002) *Trends Biochem. Sci.* **27,** 527–533
31. Uversky, V. N. (2002) *Protein Sci.* **11,** 739–756
32. Dunker, A. K., Lawson, J. D., Brown, C. J., Williams, R. M., Romero, P., Oh, J. S., Oldfield, C. J., Campen, A. M., Ratliff, C. M., Hipps, K. W., Ausio, J., Nissen, M. S., Reeves, R., Kang, C., Kissinger, C. R., Bailey, R. W., Griswold, M. D., Chiu, W., Garner, E. C., and Obradovic, Z. (2001) *J. Mol. Graph. Model.* **19,** 26–59
33. Dunker, A. K., and Obradovic, Z. (2001) *Nat. Biotechnol.* **19,** 805–806
34. Dunker, A. K., Garner, E., Guilliot, S., Romero, P., Albrecht, K., Hart, J., Obradovic, Z., Kissinger, C., and Villafranca, J. E. (1998) *Pac. Symp. Biocomput.* **3,** 473–484
35. Wright, P. E., and Dyson, H. J. (1999) *J. Mol. Biol.* **293,** 321–331
36. Uversky, V. N. (2002) *Eur. J. Biochem.* **269,** 2–12
37. Dyson, H. J., and Wright, P. E. (2002) *Curr. Opin. Struct. Biol.* **12,** 54–60
38. Buckland, R., Giraudon, P., and Wild, F. (1989) *J. Gen. Virol.* **70,** 435–441
39. Giraudon, P., Jacquier, M. F., and Wild, T. F. (1988) *Virus Res.* **10,** 137–152
40. Pothier, P., and Bour, J. B. (1997) *Med. Malad. Infect.* **11,** 592–597
41. Karlin, D., Longhi, S., Receveur, V., and Canard, B. (2002) *Virology* **296,** 251–262
42. Brizzard, B. L., Chubet, R. G., and Vizard, D. L. (1994) *BioTechniques* **16,** 730–735
43. Brinkmann, U., Mattes, R. E., and Buckel, P. (1989) *Gene* (*Amst.*) **85,** 109–114
44. Uversky, V. N. (1993) *Biochemistry* **32,** 13288–13298
45. Piotto, M., Saudek, V., and Sklenar, V. (1992) *J. Biomol. NMR* **2,** 661–665
46. Morris, M. C., Mery, J., Heitz, A., Heitz, F., and Divita, G. (1999) *J. Pept. Sci.* **5,** 263–271
47. Narayanan, T., Diat, O., and Boesecke, P. (2001) *Nucl. Instr. Methods Phys. Res. A* **467,** 1005–1009
48. Guinier, A., and Fournet, F. (1955) *Small Angle Scattering of X-rays*, Wiley Interscience, New York
49. Svergun, D. (1992) *J. Appl. Crystallogr.* **25,** 495–503
50. Bergmann, A., Fritz, G., and Glatter, O. (2000) *J. Appl. Crystallogr.* **33,** 1212–1216
51. Frank, J., Radermacher, M., Penczek, P., Zhu, J., Li, Y., Ladjadj, M., and Leith, A. (1996) *J. Struct. Biol.* **116,** 190–199
52. Cuff, J. A., Clamp, M. E., Siddiqui, A. S., Finlay, M., and Barton, G. J. (1998) *Bioinformatics* **14,** 892–893
53. Brown, C. J., Takayama, S., Campen, A. M., Vise, P., Marshall, T. W., Oldfield, C. J., Williams, C. J., and Keith Dunker, A. (2002) *J. Mol. Evol.* **55,** 104–110
54. Li, X., Romero, P., Rani, M., Dunker, A. K., and Obradovic, Z. (1999) *Genome Inform. Ser. Workshop Genome Inform.* **10,** 30–40
55. Uversky, V. N., Gillespie, J. R., and Fink, A. L. (2000) *Proteins* **41,** 415–427
56. Liu, J., Tan, H., and Rost, B. (2002) *J. Mol. Biol.* **322,** 53–64
57. Wilkins, D. K., Grimshaw, S. B., Receveur, V., Dobson, C. M., Jones, J. A., and Smith, L. J. (1999) *Biochemistry* **38,** 16424–16431
58. Hua, Q. X., Jia, W. H., Bullock, B. P., Habener, J. F., and Weiss, M. A. (1998) *Biochemistry* **37,** 5858–5866
59. Van Hoy, M., Leuther, K. K., Kodadek, T., and Johnston, S. A. (1993) *Cell* **72,** 587–594
60. Receveur, V., Durand, D., Desmadril, M., and Calmettes, P. (1998) *FEBS Lett.* **426,** 57–61
61. Russo, D., Durand, D., Calmettes, P., and Desmadril, M. (2001) *Biochemistry* **40,** 3958–3966
62. Panick, G., Malessa, R., Winter, R., Rapp, G., Frye, K. J., and Royer, C. A. (1998) *J. Mol. Biol.* **275,** 389–402
63. Perez, J., Vachette, P., Russo, D., Desmadril, M., and Durand, D. (2001) *J. Mol. Biol.* **308,** 721–743
64. Konno, T., Kamatari, Y. O., Kataoka, M., and Akasaka, K. (1997) *Protein Sci.* **6,** 2242–2249
65. Glatter, O., and Kratzy, O. (1982) *Small Angle X-ray Scattering*, Academic Press, London
66. Finch, J. T., and Gibbs, A. J. (1970) *J. Gen. Virol.* **6,** 141–150
67. Schoehn, G., Iseni, F., Mavrakis, M., Blondel, D., and Ruigrok, R. W. (2001) *J. Virol.* **75,** 490–498
68. Liston, P., DiFlumeri, C., and Briedis, D. J. (1995) *Virus Res.* **38,** 241–259
69. Tarbouriech, N., Curran, J., Ebel, C., Ruigrok, R. W., and Burmeister, W. P. (2000) *Virology* **266,** 99–109
70. Tarbouriech, N., Curran, J., Ruigrok, R. W., and Burmeister, W. P. (2000) *Nat. Struct. Biol.* **7,** 777–781
71. Marion, D., Tarbouriech, N., Ruigrok, R. W., Burmeister, W. P., and Blanchard, L. (2001) *J. Biomol. NMR* **21,** 75–76
72. Diamond, R. (1974) *J. Mol. Biol.* **82,** 371–391
73. Dedmon, M. M., Patel, C. N., Young, G. B., and Pielak, G. J. (2002) *Proc. Natl. Acad. Sci. U. S. A.* **99,** 12681–12684
74. Daughdrill, G. W., Hanely, L. J., and Dahlquist, F. W. (1998) *Biochemistry* **37,** 1076–1082
75. Gast, K., Damaschun, H., Misselwitz, R., Muller-Frohne, M., Zirwer, D., and Damaschun, G. (1994) *Eur. Biophys. J.* **23,** 297–305
76. De, B. P., and Banerjee, A. K. (1999) *Microsc. Res. Tech.* **47,** 114–123
77. Moyer, S. A., Baker, S. C., and Horikami, S. M. (1990) *J. Gen. Virol.* **71,** 775–783
78. Egelman, E. H., Wu, S. S., Amrein, M., Portner, A., and Murti, G. (1989) *J. Virol.* **63,** 2233–2243
79. Curran, J., Pelet, T., and Kolakofsky, D. (1994) *Virology* **202,** 875–884
80. Curran, J., Boeck, R., Lin-Marq, N., Lupas, A., and Kolakofsky, D. (1995) *Virology* **214,** 139–149
81. ten Oever, B. R., Servant, M. J., Grandvaux, N., Lin, R., and Hiscott, J. (2002) *J. Virol.* **76,** 3659–3669
82. Marie, J. C., Kehren, J., Trescol-Biemont, M. C., Evlashev, A., Valentin, H., Walzer, T., Tedone, R., Loveland, B., Nicolas, J. F., Rabourdin-Combe, C., and Horvat, B. (2001) *Immunity* **14,** 69–79
83. Ravanel, K., Castelle, C., Defrance, T., Wild, T. F., Charron, D., Lotteau, V., and Rabourdin-Combe, C. (1997) *J. Exp. Med.* **186,** 269–278